Springer

Acta Mechanica Sinica

CrossMark click for updates

• RESEARCH PAPER •

Acta Mech. Sin., Vol. 40, 523370 (2024)
https://doi.org/10.1007/s10409-024-23370-x

# Negative Poisson's ratio locally resonant seismic metamaterials vibration isolation barrier

Haibin Ding[1,2], Nianyong Huang[1,2], Muhammad[3,4], Changjie Xu[1,2], and Lihong Tong[1,2*]

[1]*State Key Laboratory of Performance Monitoring and Protecting of Rail Transit Infrastructure, Nanchang 330013, China;*
[2]*Institute of Geotechnical Engineering, School of Civil Engineering and Architecture, East China Jiaotong University, Nanchang 330013, China;*
[3]*Department of Mechanical, Manufacturing and Biomedical Engineering, Trinity College Dublin, Dublin D02PN40, Ireland;*
[4]*Department of Mechanical Engineering, University of Galway, University Road, Galway H91 HX31, Ireland*

Received November 9, 2023; accepted January 31, 2024; published online May 7, 2024

In recent decades, the application of seismic metamaterials to protect civil infrastructures being free of the damage of earthquakes has been attracting extensive attention. Specifically, the proposed locally resonant seismic metamaterials provide the probability of isolating the low-frequency seismic wave using a small-size isolation barrier. However, in previous studies, the energy absorption properties of locally resonant seismic metamaterials remain one of the least understood aspects of isolation. Benefit from the fascinating energy absorption characteristic of negative Poisson ratio (NPR) metamaterial, we creatively design a new seismic metamaterial structure by assembling the locally resonant seismic metamaterial and NPR metamaterial, to isolate seismic waves. The sound cone technique combining the transmission spectrum is employed to identify the surface wave from the hybrid waves. The generation mechanism of frequency bandgap and the isolation effectiveness of the proposed seismic metamaterial are discussed in detail. The results indicate that the generation of ultra-low and ultra-wide frequency bandgap with the range of 0.65 Hz-18.9 Hz is attributed to the locally resonant and energy absorption of the proposed seismic metamaterial structure and the excellent isolation effect is achieved by transforming the surface wave into the bulk wave. The frequency bandgap narrows as the distance increases between each resonator. In addition, the mechanical properties of the NPR bearing, such as the Poisson ratio, mass density, and elastic modulus, have remarkable impact on the frequency bandgap, especially on the upper bound frequency. In practical engineering, the NPR bearing with a low Poisson ratio, small mass density, and high elastic modulus is suggested for the design of the NPR locally resonant seismic metamaterial structures. Time domain analysis for the practical seismic wave verifies that the proposed seismic metamaterial has a promising application in isolating ultra-low and ultra-wide seismic waves, with the isolation effectiveness larger than 70%. This work contributes a new locally resonance seismic metamaterial design idea for isolating and adjusting the low-frequency seismic wave.

**Seismic metamaterials, Locally resonant, Negative Poisson ratio (NPR), Seismic waves, Frequency bandgap, Vibration isolation barrier**

**Citation:** H. Ding, N. Huang, Muhammad, C. Xu, and L. Tong, Negative Poisson's ratio locally resonant seismic metamaterials vibration isolation barrier, Acta Mech. Sin. 40, 523370 (2024), https://doi.org/10.1007/s10409-024-23370-x

## 1. Introduction

Earthquakes consistently threaten the security of humans and building structures, damaging the socio-economic system and causing a catastrophe, such as the Wenchuan earthquake in China [1], the Niigataken-Chuetus earthquake in Japan [2] and recent earthquakes in Turkey and Syria [3]. Preventing civil infrastructures from damages caused by earthquakes to protect people's lives and property is of paramount significance. The studies of periodic arrays of piles [4], wave-impeding blocks [5], and building base-isolation systems [6], as well as the seismic metamaterial barriers on isolating civil infrastructures from earthquakes,

*Corresponding author. E-mail address: lhtong@ecjtu.edu.cn (Lihong Tong)
Executive Editor: Guilin Wen

have been reported [7].

Metamaterial is manually engineered composite periodic/aperiodic structures with some unusual physical phenomena and wave dispersion properties that are inconceivable from naturally occurring materials. The main property of interest includes frequency bandgap [8] and frequency range where wave propagation is impeded. Likewise, locally resonant metamaterials also exhibit negative mass density [9], negative moduli [10], and negative refraction [11] properties near resonance frequencies. This new class of functional materials also exhibits negative Poisson's ratio property [12], leading to the discovery of a new class of auxetic metamaterial [13].

In recent years, seismic metamaterial to shield critical civil infrastructures from earthquakes has been extensively studied, achieving fascinating results. Particularly, a full-scale field test with a periodic array of holes as phononic barriers has achieved artificial wave isolation around 50 Hz [14]. This large-scale experiment effectively verified the practical value of seismic metamaterials for seismic wave isolation. However, the frequency of the seismic waves is usually lower than 20 Hz, and further study on the seismic metamaterial needs to be carried out to achieve low-frequency seismic wave isolation. According to the occurring mechanism of frequency bandgaps, seismic metamaterials can be mainly divided into two types: Bragg scattering and locally resonant metamaterials [7]. For the Bragg scattering mechanism, the frequency bandgap is generated from the reflection, refraction, and transmission of the elastic waves in the periodic structure, which requires that the size of the isolation structure is of the same order of magnitude as the wavelength of propagating wave [15,16]. For instance, the periodic row of piles [17], periodic wall [18], and periodic foundation [19,20], and so on. The enormous size demands limit the development of the Bragg scattering seismic metamaterials in practical engineering. However, for the locally resonant seismic metamaterials, the frequency bandgap is generated by the resonant effect of the resonator [21,22], which provides the possibility for low-frequency subwavelength seismic isolation by small-size engineered barriers. Based on the locally resonant mechanism, the cylindrical pillars were put on the surface of the semi-infinite substrate periodicity to obtain the locally resonant metasurface and achieved a subwavelength frequency bandgap than Bragg scattering phononic crystals [23]. Subsequently, some studies have considered the H-shaped and built-up steel sections as seismic metamaterials for surface wave attenuation [24,25]. The low-frequency bandgap was observed by the simulations in COMSOL Multiphysics.

In 2016, an interesting phenomenon was noted: the Rayleigh waves passing through natural forests can convert to shear waves traveling downward, and the disordered and gradient arrangement of the resonators was proposed subsequently [26,27]. This phenomenon provides a new idea to apply the locally resonant metamaterials in seismic wave diversion. Recently, the influence of the distribution of branches in the forest, the angle between the branches, and the thickness of the branches on the isolation effect were discussed in detail [28,29], and the analytical solution for forest trees as a natural metamaterial using a closed-form Green's function method is also obtained in the stratified soils [30]. Inspired by the work of Colombi et al. [26,27], a new locally resonant structure compositing the steel cylindrical, elastic bearings, and concrete hollow tube was proposed [21,31]. The analysis indicated that the frequency bandgap of this structure is 5 Hz-7.5 Hz. Subsequently, an improved resonant structure with a frequency bandgap of 6.72 Hz-20 Hz was proposed [22]. Recently, the laboratory test was further designed to verify the effectiveness of the locally resonant seismic metamaterials [32]. In addition, numerous studies have investigated the locally resonant seismic metamaterial [33,34]. Although locally resonance seismic metamaterials have been investigated widely, and many fascinating conclusions were obtained, the energy-absorbing characteristic of the local resonator is not considered in current research.

Negative Poisson ratio (NPR) metamaterials are artificial materials with special mechanical properties that expand laterally under tensile action and contract under uniaxial compression. Earlier studies indicate NPR materials have stronger energy-absorbing characteristics [35-38] than positive Poisson ratio materials. Previously, the NPR structures were mainly considered energy-absorbing devices [37,38], such as vibration isolation bases [39], which mainly utilize the great energy-absorbing characteristics of NPR metamaterial. Inspired by the NPR metamaterials, The first auxetic-like seismic metamaterial was designed [39] with a size of 10 m × 10 m, and the frequency bandgap of that structure is 30 Hz-60 Hz. Recently, a new seismic metamaterial was designed, compositing the auxetic foam and square steel column with a structure size of 10 m × 20 m [40]. The results indicate that the elastic modulus, Poisson ratio, and density of the auxetic foam strongly influence the frequency bandgap. The above proposed NPR metamaterial used in environmental isolation has an enormous geometric size, limiting practical engineering implementation. Therefore, it is necessary to develop a small vibration isolation barrier to isolate the low-frequency wave.

Inspired by the above investigation, a novel NPR locally resonant seismic metamaterial combining the advantageous characteristics of locally resonant seismic metamaterial and NPR metamaterial to isolate the Rayleigh wave is proposed in this work. Each resonant unit contains a heavy square steel column encased in a concrete hollow tube and suspended by the NPR metamaterial. The resonant unit is

periodically arranged in a half-infinite subgrade to form the NPR locally resonant seismic metamaterial isolation barrier. The frequency bandgap of the novel metamaterial is obtained using eigenfrequency analysis for the cell structure. Subsequently, the vibration reduction and isolation mechanism are discussed in detail. The results of this work provide a new design idea to isolate low-frequency seismic waves.

## 2. NPR local resonant seismic metamaterials and theoretical formwork

### 2.1 Designing of NPR resonant seismic metamaterials

The local resonator designed in this work is comprised of two rectangular concrete slabs, a steel column, and two NPR bearings. The geometrical configurations and spatial relationship of these components are shown in Fig. 1(b). These components are encapsulated by a concrete square box to create the local resonator. By embedding the resonator into the semi-infinite sedimentary soil periodically, the seismic metamaterial barrier is formed. In Ref. [31], it is anticipated that the surface wave can be converted to bulk waves, realizing the function of isolation, as shown in Fig. 1(a). The geometrical parameters of the resonator are shown in Fig. 1(b), in which $l_c$ and $t_c$ represent the length and thickness of rectangle concrete slabs, $h$ and $l_N$ represent the height and length of steel column, $r_c$ is the radius of the four cylinders embedded into the corners of the steel column, and $t_N$ is the thickness of NPR bearing.

### 2.2 Dispersion theory for periodic structures

In this work, the semi-infinite sedimentary soil is assumed to be a perfectly elastic, homogeneous, and isotropic single-phase medium for simple analysis. Thus, the governing equation can be given as [41,42]

$$(\lambda+\mu)\nabla(\nabla\cdot\mathbf{u})+\mu\nabla^2\mathbf{u}=\rho\ddot{\mathbf{u}}, \tag{1}$$

where $\lambda$ is the Lame constant; $\mu$ is the shear modulus; $\rho$ is the mass density; $\nabla$ is the gradient operator; $\nabla\cdot$ is the divergence operator; $\nabla^2$ is the Laplace operator. To study wave propagation in an infinite space, the Floquet-Bloch periodicity theory, which can be expressed as [16], is employed.

$$\begin{aligned}\mathbf{u}(\mathbf{r}+\mathbf{a},t)&=\mathbf{u}_k(\mathbf{r}+\mathbf{a})\mathrm{e}^{\mathrm{i}(\mathbf{k}\cdot(\mathbf{r}+\mathbf{a})-\omega t)}\\&=\mathrm{e}^{\mathrm{i}\mathbf{k}\cdot\mathbf{a}}\mathbf{u}_k(\mathbf{r})\mathrm{e}^{\mathrm{i}(\mathbf{k}\cdot\mathbf{r}-\omega t)}=\mathrm{e}^{\mathrm{i}\mathbf{k}\cdot\mathbf{a}}\mathbf{u}(\mathbf{r},t),\end{aligned} \tag{2}$$

In Eq. (2), we can find that the phase difference between the input wave and the output wave is $\mathbf{k}\cdot\mathbf{a}$, which is a scalar parameter. By virtue of this characteristic, the eigenvalue problem in an infinite domain can be simplified to a finite domain problem by applying the periodic displacement boundary condition on the unit cell. Therefore, the dispersion relation can be obtained by submitting Eq. (2) into Eq. (1), which can be shown as

$$\left(\mathbf{\Omega}(\mathbf{k})-\omega^2\mathbf{M}\right)\cdot\mathbf{U}=0, \tag{3}$$

where $\mathbf{\Omega}(\mathbf{k})$ is the stiffness matrix related to the wave vector $\mathbf{k}$; $\mathbf{M}$ is the mass matrix; $\mathbf{U}$ is the displacement vector. For a given wave number $\mathbf{k}$, the eigenfrequency $\omega$ can be solved using the modal analysis method. Considering the complexity of Eq. (3), the commercial FEM software COMSOL Multiphysics is used to solve this equation to obtain the dispersion curve, as it can solve the eigenvalue problems with complex boundary conditions [43]. To obtain the frequency bandgap, the unit cell model is established for eigenfrequency analysis, and the wave vector $\mathbf{k}$ sweeps through the first irreducible Brillouin zone, as shown in Fig. 1(c). If the eigenfrequency exists for a given wave vector $\mathbf{k}$, indicating that the wave can propagate through the seismic metamaterial. Conversely, if no eigenfrequency exists for the given wave vector $\mathbf{k}$, it implies that the wave cannot pass through the structure, and the corresponding frequency range is termed a frequency bandgap. A more detailed presentation will be provided in Sect. 3. Note that, according to the work of Palermo et al. [21], the resonators are viewed as the stress boundary on the ground surface. Then Eq. (3) can be simplified in the following form, only considering the vertical and horizontal vibration subjected to Rayleigh wave.

$$\begin{aligned}&\left(2-\frac{\omega^2}{k^2c_s^2}\right)^2-4\sqrt{1-\frac{\omega^2}{k^2c_L^2}}\sqrt{1-\frac{\omega^2}{k^2c_s^2}}\\&+\frac{m\omega^4}{Ac_s^4\rho k^3}\frac{\omega_v^2}{\omega_v^2-\omega^2}\sqrt{1-\frac{\omega^2}{k^2c_L^2}}\\&+\frac{m\omega^4}{Ac_s^4\rho k^3}\frac{\omega_h^2}{\omega_h^2-\omega^2}\sqrt{1-\frac{\omega^2}{k^2c_L^2}}=0,\end{aligned} \tag{4}$$

where $\omega_v=\sqrt{K_v/m}$ and $\omega_h=\sqrt{K_h/m}$ are respectively the vertical and horizontal angular frequency of the resonator; $K_v=2M_bA_b/h_b$ and $K_h=2G_bA_b/h_b$ are respectively the stiffness in vertical and horizontal direction; $M_b$ and $G_b$ are respectively the elastic modulus and shear modulus of NPR bearing; $A_b$ and $h_b$ respectively the area and height of NPR bearing; $m=A_rh_r\rho_s$ is the effective mass of the resonator; $A_r$, $h_r$, and $\rho_s$ are the section area, height, and mass of NPR bearing. $c_s$ and $c_L$ are the P wave and SV wave velocity in semi-infinite sedimentary soil; $A$ is the average action area; $\rho$ is the density of sedimentary soil. The dispersion curve can be obtained by solving Eq. (4).

### 2.3 Surface wave identification and model validation

It should be noted that the dispersion relations obtained from

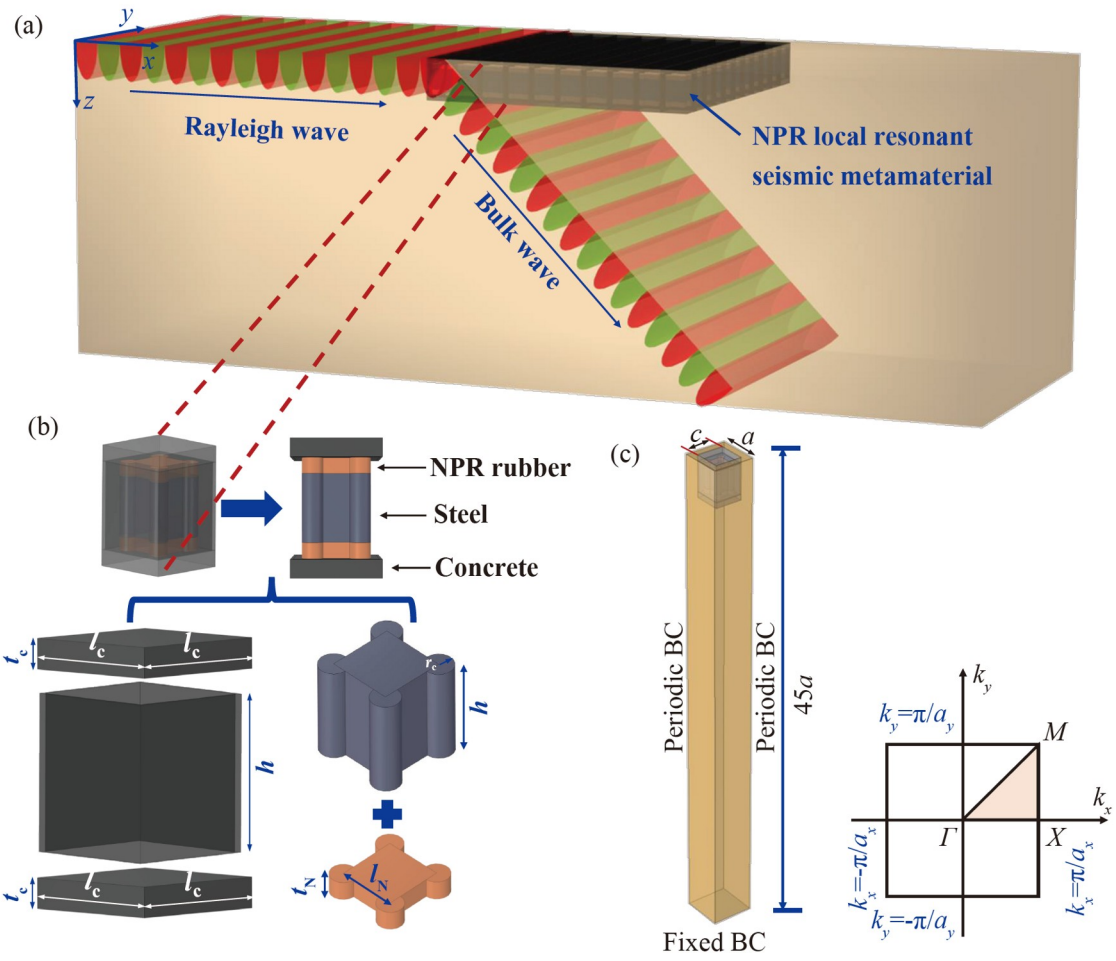


**Figure 1** Schematic diagram of the NPR locally resonator seismic metamaterial. (a) Designing of NPR locally resonant seismic metamaterial and converting the Rayleigh wave into bulk waves; (b) the components of the NPR local resonator; (c) the unit cell and first irreducible zone.

simulations in COMSOL Multiphysics include both surface wave modes and body wave modes. To clearly analyze the isolation effect of the seismic metamaterial, it should identify the surface wave from the mixed modes should be identified. According to the previous work, two methods are widely used to identify the surface wave modes, i.e., the sound cone technique [44] and the strain energy method [45]. The sound cone technique limited by the sound line is employed in the present work. The sound line corresponds to the shear wave in sedimentary soil along a different direction, which is governed by the formula of $\omega = \mathbf{k} \cdot c_s$, in which $c_s = \sqrt{\mu / \rho}$ is the shear wave velocity, $\mu$ and $\rho$ are respectively the shear modulus and density of sedimentary soil. The sound cone criterion is based on the principle that the surface wave velocity is less than the body wave, and the velocity of the shear wave in the body wave is less than the longitudinal wave velocity. Thus, the region below the sound cone only contains the surface modes.

In order to verify the accuracy of the sound cone technique, the seismic metamaterial and the numerical model proposed by Zeng et al. [46] are re-conducted. The geometric dimension, boundary conditions, and material parameters are completely consistent with the work of Zeng et al. [46]. The material properties are exhibited in the illustration of Fig. 2. The strain energy method proposed by Pu and Shi [45] is also presented for comparison. According to the work of Pu and Shi [45], the strain energy method can be described by an energy distribution parameter, which is defined as

$$\xi = \frac{\int_{(2\lambda)z} W_\varepsilon \, \mathrm{d}\Omega}{h \int W_\varepsilon \, \mathrm{d}\Omega}, \tag{5}$$

where $\Omega$ is the whole volume of the unit cell; $W_\varepsilon$ is the strain energy; $h$ is the height of the unit cell; $z$ is the influence depth of the surface wave, which can be fixed as $2\lambda$; $\lambda$ is the wavelength of the minimum frequency for the considered surface wave. It is obvious that the value of the energy distribution parameter determined by Eq. (5) is located in the range of 0 to 1. As we all know, the energy of surface waves decays exponentially along the depth. Thus, the waves are surface modes when the energy distribution parameter approaches 1. As suggested by most of the re-

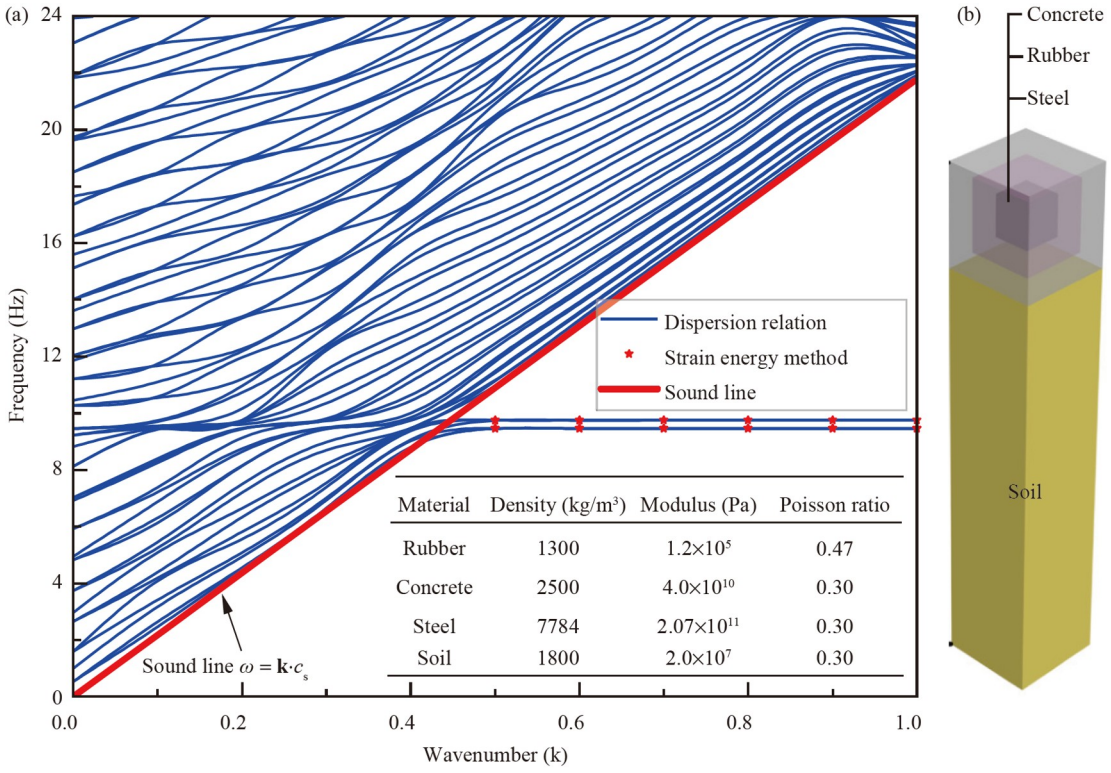


**Figure 2** Verify the sound cone method by reconsidering the work of Zeng et al. [46]. (a) Dispersion curve and surface wave identification; (b) unit cell for eigenfrequency analysis.

searchers, $\xi > 0.9$ can be taken as the surface wave identification criterion. The dispersion curves for the seismic metamaterial are shown in Fig. 2, in which the surface wave identification results by sound cone technique and strain energy method are also presented. Obviously, the results of the sound cone and strain energy are consistent, which indicates the effectiveness of the sound cone method.

## 3. Results and discussion

### 3.1 Degree of attenuation

To evaluate the degree of attenuation of the NPR local resonant seismic metamaterial for surface wave, a 3D finite element model is established. As shown in Fig. 3, the front view and planform of the 3D finite element model are presented. In the *y*-direction, the width of the 3D model is equal to one lattice constant. In practical engineering, all structures are finite, and the degree of attenuation analysis is based on finite structures. In this work, 30 resonators were installed on the surface of the ground. The length and height of the whole finite model are $l = 131a$ and $h = 45a$, respectively. The low-reflection boundary condition conditions are applied on the model's left, right, and bottom surfaces to eliminate the influences of reflected waves. The fixed boundary condition is also set on the bottom surface of the model for the stability of the system. In addition, to improve the computational efficiency, the Floquet-Bloch periodicity boundary condition is applied to the *y*-direction to simulate the periodicity structure. The unit load was used to generate the Rayleigh wave in a half-infinite foundation, and the distance to the left boundary of the finite element model is $l_1 = 2a$. The output area with the length of $l_4 = 8a$, as shown in Fig. 3, is used to record the output signal for transmission spectrum analysis. The load source distance of the NPR locally resonant seismic metamaterial is $l_2 = 68.5a$, which should be large enough to ensure only the surface wave interaction with the seismic metamaterial. The output area distances of the seismic metamaterial and the right side of the finite model are $l_3 = 10.5a$ and $l_5 = 12a$, respectively. To evaluate the degree of attenuation of the seismic metamaterial, it is necessary to introduce the amplitude reduction

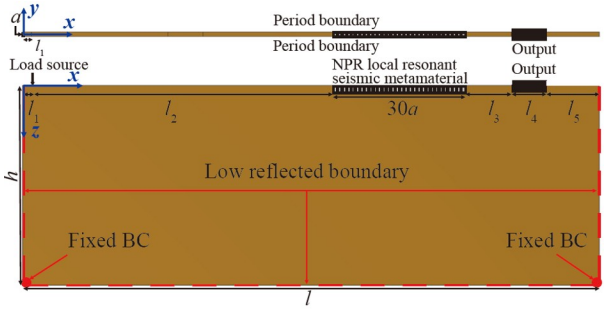


**Figure 3** Schematic of finite element model.

spectrum (ARS), which is defined as

$$ARS = 20\log_{10}\left(\overline{A}_1 / \overline{A}_0\right), \tag{6}$$

in which $\overline{A}_1$ and $\overline{A}_0$ are the average displacement amplitudes of the output area with and without seismic metamaterial, respectively. Obviously, if the seismic metamaterial works, the value of ARS is below 0 dB.

### 3.2 Frequency bandgap for the seismic metamaterial

To obtain the frequency bandgap of the novel seismic metamaterial, The unit cell model in Fig. 1(c) is taken for analysis. As indicated above, the frequency bandgap can be obtained by sweeping the wave vector **k** from $\Gamma \rightarrow X \rightarrow M$ in the first irreducible Brillouin zone due to the symmetry of the structure. The unit cell has a lattice constant $a$, and all other geometric parameters are mentioned with reference to it. To simulate the periodic structures, the Floquet-Bloch periodicity condition is implemented on all vertical sides [47]. In order to guarantee only the surface on the ground surface, the fixed boundary condition is imposed at the bottom, and free conditions are applied on the ground surface of the unit cell structure. The unit cell height in the $z$-direction should be enough height to allow the decoupling of the Lamb mode into surface wave modes [43]. In this work, $h = 45a$ is selected to satisfy this requirement. To comprehensively consider the computational accuracy and efficiency, the free tetrahedral mesh with the largest size and the smallest size of 0.3 m is applied, where is the wavelength of the Rayleigh wave which is required to be much larger than the lattice size. The geometric dimension and the physical parameters of the local resonator are listed in Table 1. Obviously, the total height of the resonator is 2.6 m.

To investigate the influence of the soil among the periodically arranged NPR locally resonators on the frequency bandgap of seismic metamaterial, four types of resonators spacing with $a$ = 1.7 m, 2.3 m, 3.0 m, and 3.4 m keeping $c$ = 1.7 m as a constant was selected for eigenfrequency analysis. Note that when the lattice constant $a$ = 1.7 m, the seismic metamaterial then becomes a continuous periodic structure with no soil among the resonators. In order to validate that the seismic metamaterial can attenuate the surface wave in the frequency bandgap range, the corresponding ARS was calculated using the finite element model of Fig. 3 by sweeping the frequency from 0.1 Hz-20 Hz with the step of 0.1 Hz. The dispersion curves and the ARS for the four types of resonator spacing are shown in Fig. 4. The partially enlarged drawing is also given for more clearly observing the relationship between the sound cone line and the dispersion curves.

Figure 4(a) shows the dispersion relations and ARS of the NPR locally resonant seismic metamaterial with the lattice constant $a$ = 1.7 m. Corresponding to the dispersion relations in the first irreducible Brillouin zone, the highest frequency of the sound line is 18.9 Hz, and the frequency bandgap below the sound line is considered in this work. A significant attenuation degree for the surface wave below the highest frequency is achieved. Whereas beyond the highest frequency considered in this work, the attenuation degree is still remarkable because the wavelength decreased with increasing the input frequency, and the Bragg scattering is generated between the seismic metamaterial and Rayleigh wave. Note that the calculation results of ARS within the ultra-low frequency range are inaccurate because the wavelength is much larger than the seismic metamaterial.

Figure 4(b)-(d) show the dispersion relations for lattice constant $a$ = 2.3 m, 3.0 m, and 3.4 m, which correspond to the condition that the distance between each resonator is 0.6 m, 1.3 m, and 1.7 m, respectively. In the enlarged drawing, the sound line almost overlaps with the dispersion curves for lattice constant $a$ = 2.3 m. In fact, part of the dispersion curves is below the sound line, such as the frequency range of 0.65 Hz-3.64 Hz and 0.65 Hz-5.05 Hz for $a$ = 3.0 m and 3.4 m, respectively, which means no Bandgaps (BGs) exist in that frequency range. Moreover, from the ARS in Fig. 4(c) and (d), attenuation is achieved in the frequency range of 3.64 Hz-10.7 Hz and 5.05 Hz-9.4 Hz. Thus, the frequency bandgap for the four types of resonator distances of the seismic metamaterial is 0.65 Hz-18.9 Hz, 0.65 Hz-13.9 Hz, 3.64 Hz-10.7 Hz, and 5.05 Hz-9.4 Hz, respectively. Obviously, with increasing the distance of each resonator, the highest frequency decreases gradually, whereas the lower frequency increases when the distance reaches a critical value. As the above discussion, the BGs become smaller as the distance between each resonator increases, which demonstrates that the distance increase is not conducive to generating broad BGs. Thus, we are only focused on the case of $a$ = 1.7 m in our following analysis.

**Table 1** Geometric dimension and material parameters

| Materials | | Length/radius (m) | Height (m) | Elastic modulus $E$ (MPa) | Poisson's ratio $v$ | Density $\rho$ (kg/m$^3$) |
|---|---|---|---|---|---|---|
| Sedimentary soil | | – | – | 20 | 0.35 | 1800 |
| Steel column | Square column | 0.9 | 1.3 | 210000 | 0.3 | 7800 |
| | Cylinder | 0.3 (radius) | 1.3 | 210000 | 0.3 | 7800 |
| NPR bearing | Square column | 0.9 | 0.3 | 0.025 | −0.1 | 120 |
| | Cylinder | 0.3 (radius) | 0.3 | 0.025 | −0.1 | 120 |
| Concrete slabs | | 1.7 | 0.35 | 40000 | 0.2 | 2500 |

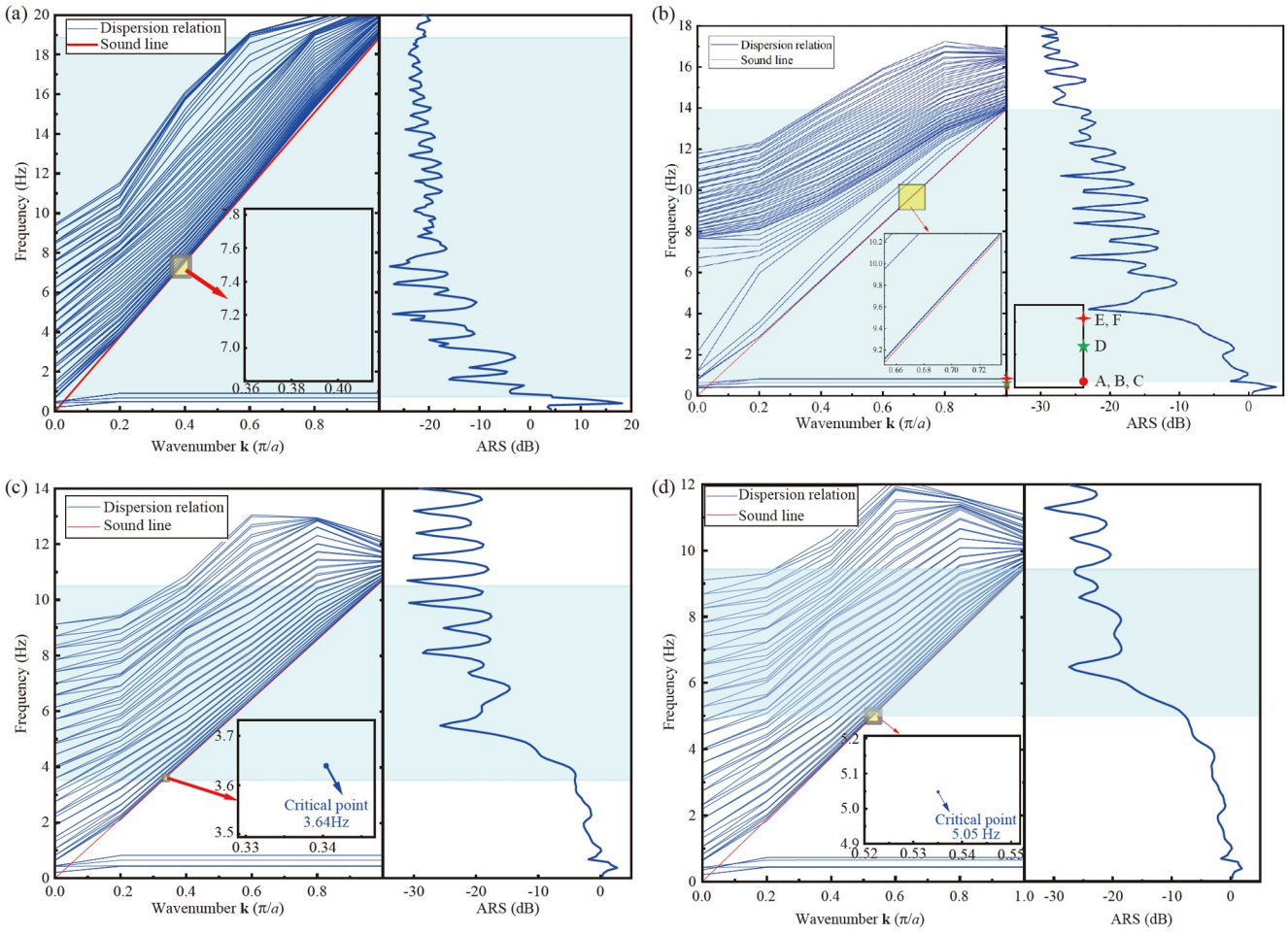


**Figure 4** Dispersion curves and ARS of the NPR locally resonant seismic metamaterial. (a) $a$ = 1.7 m; (b) $a$ = 2.3 m; (c) $a$ = 3.0 m; (d) $a$ = 3.4 m.

To illustrate the generation mechanism of the frequency bandgap for the NPR locally resonant seismic metamaterials, the vibration displacement modes corresponding to points A-F marked in Fig. 4(b) are shown in Fig. 5. The wave vector of points A-F is 1 with the angle frequency of 0.427 Hz, 0.444 Hz, 0.445 Hz, 0.649 Hz, 0.822 Hz, and 0.822 Hz, respectively. Note that points A, B, and C almost overlap, as well as points E and F. In the modal diagram, the black arrows represent the vibration direction of the displacement field, and the color bar on the right side is the normalized displacement amplitude. For clearly observing the vibration modes of the proposed seismic metamaterial, the 3D deformation nephogram at points A-F is presented in Fig. 5. Point A is the lowest modal, which rotates around the geometric center of the resonator, and the energy of the surface wave is dissipated by this method. In addition, the displacement uniform distribution along the $z$-direction is independent of the height of the steel column. Note that the steel column in the resonator has significant displacement relative to the soil while weak for the concrete box. The points B and C only present considerable displacement in the horizontal direction. The steel column in the resonator vibrates vertically significantly at point D, which results in vertical resonance, and the energy is mainly concentrated in the steel column. Considering the elliptical motion pattern of the Rayleigh wave, it is not difficult to infer that point D is the main reason for the Rayleigh wave bandgap. In addition, according to Eq. (4), the vertical resonance frequency of the structure is $\omega_{\mathrm{v}} = \sqrt{K_{\mathrm{v}}/m}$, which indicates that $f_{\mathrm{v}} = \frac{1}{2\pi}\sqrt{\frac{K_{\mathrm{v}}}{m}}$. The resonance frequency of $f_{\mathrm{v}}$=0.645 Hz can be obtained by taking the parameters of the resonator into the above equation. The theoretical result is approximately equal to the numerical result at point D of 0.649 Hz, verifying that point D is the Rayleigh wave mode. Points E and F have significant rotational displacement along the $y$-axis and $x$-axis. Distinctly, the displacement field in the resonator mainly concentrates in the steel column at points A to F, which demonstrates that the generation mechanism of the frequency bandgap is based on the locally resonant mechanism.

From the above analysis, an ultra-low and ultra-wide surface wave bandgap is realized using the NPR locally resonant seismic metamaterial. The generation mechanism

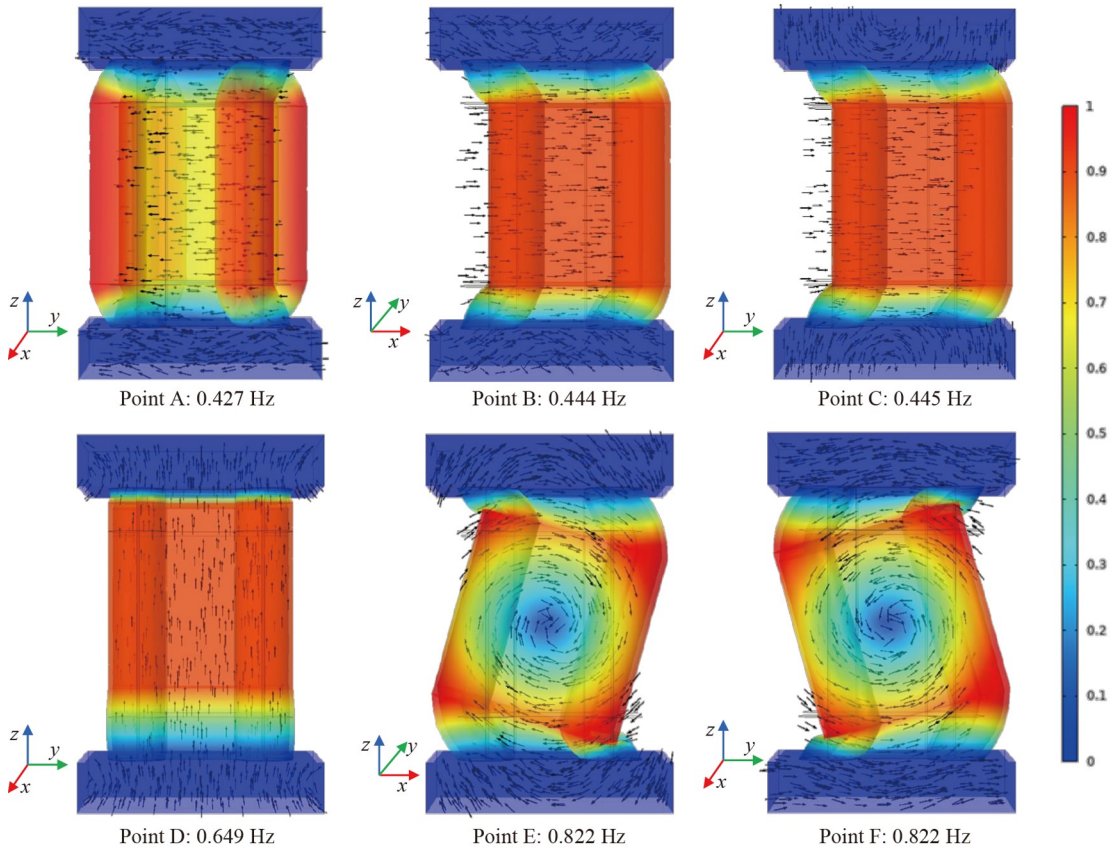


**Figure 5** Vibration displacement modes of the points A-F marked in Fig. 4(b).

can be attributed to two aspects: (1) strong coupling resonance between the seismic metamaterial and the Rayleigh wave, and the Rayleigh wave transform into the bulk wave, which has been confirmed by many researchers [48-50]; (2) the excellent energy absorption property [51,52] of the NPR materials promotes the generation of broad BGs.

### 3.3 Effect of the mechanical property of NPR material

To further investigate the influence of NPR material on the frequency bandgap. The frequency bandgap varies with the Poisson ratio, mass density, and elastic modulus of the NPR material are discussed. The height of the NPR material in Fig. 6(a)-(c) are respectively 0.3 m, 0.5 m, and 0.7 m, keeping the total height of the resonant as 2.6 m. Note that the various heights of NPR material mean the reduction in effective mass due to the total height of the resonant as constants. It is observed that the upper bound frequency (UBF) has a significant variation with the Poisson ratio, mass density, and elastic modulus of NPR material. The UBF decreases shapely with the Poisson ratio and mass density while increasing with the elastic modulus of NPR material, i.e., the UBF decreases from 18.7 Hz to 11.6 Hz with increasing the NPR value. However, the lower bound frequency (LBF) decreases with the increase of the Poisson ratio and increases with the increase of the elastic modulus while almost unchanged with mass density. In addition, with increasing the height of NPR material, the UBF decreases shapely due to the decrease of effective mass. In general, the density, Poisson ratio, and elastic modulus have significant influences on the frequency bandgap, especially on the UBF of the bandgap. Therefore, in practical engineering, NPR material with low Poisson value, low mass density, and high elastic modulus should be chosen to generate the ultra-low and ultra-wide frequency bandgap.

### 3.4 Frequency domain analysis

To validate the isolation effectiveness of the NPR local resonant seismic metamaterial, we sweep the frequency from 0.1 Hz to 20 Hz in the frequency domain range. The finite element model shown in Fig. 3 is also used in this section for frequency domain analysis, and the parameters are consistent with those presented in Sect. 3.2. The displacement field distribution at a frequency of 1.4 Hz, 3.0 Hz, 6.0 Hz, 10 Hz, 14 Hz, and 18 Hz, which is located in the range of frequency bandgap, is shown in Fig. 7. Obviously, the energy of the incident wave is mainly concentrated on the ground surface, which indicates that the main mode is the surface mode. It is observed that the surface wave

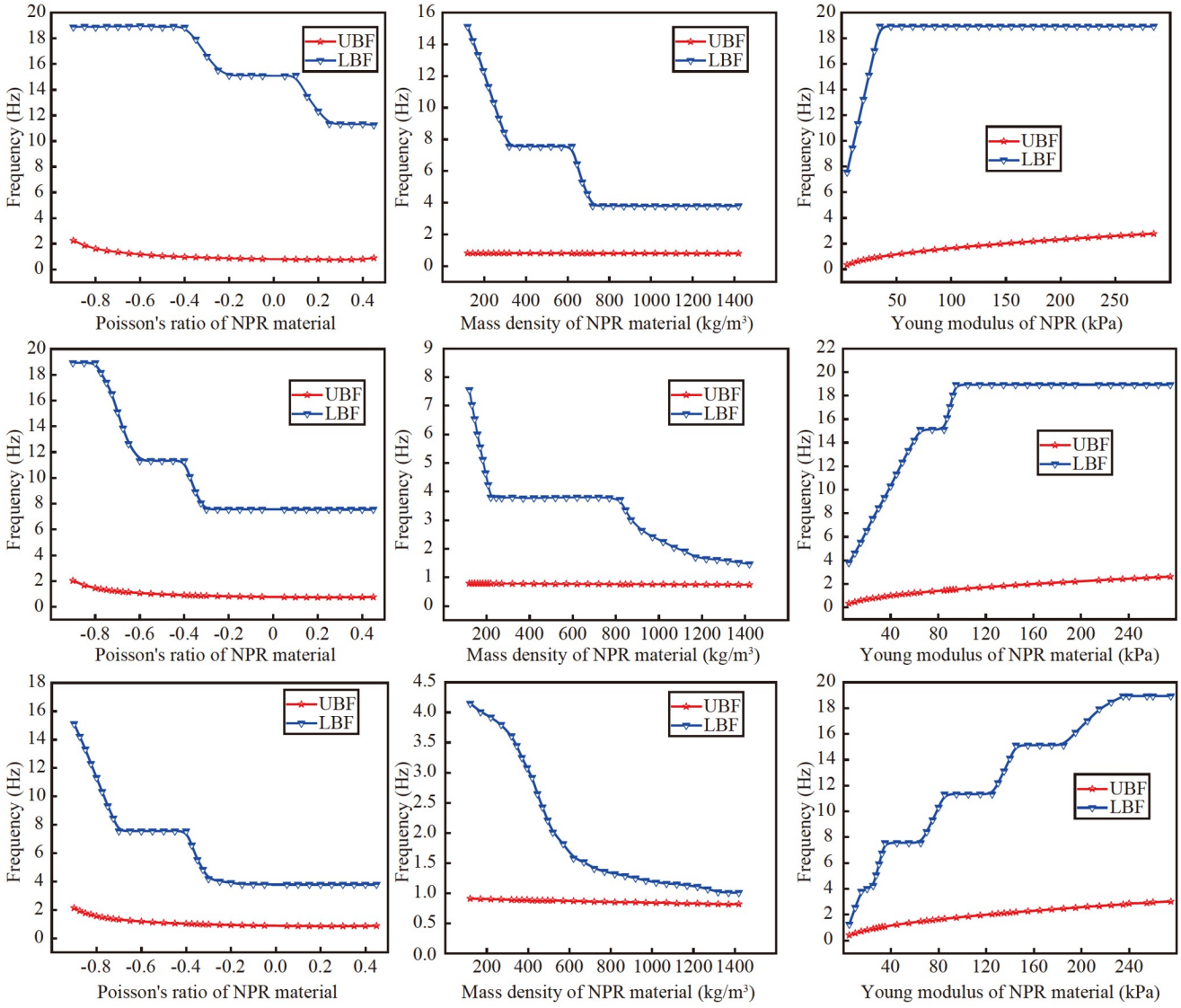


**Figure 6** The influences of properties of NPR material on the frequency bandgap. The height of NPR bearing is (a) 0.3 m, (b) 0.5 m, and (c) 0.7 m.

transforms into the bulk wave when the frequency falls into the frequency bandgaps, which proves the isolation effectiveness of the NPR local resonant seismic metamaterial.

### 3.5 Performances in isolating the real earthquake spectrum

In the previous discussion, the isolation mechanism of the NPR locally Resonant seismic is elaborated. In this section, we study the performances of this metamaterial barrier in isolating the earthquake spectrum. Three real earthquake spectra (the Kobe earthquake in Japan, the Tsukidate earthquake in Japan, and the Jiashi earthquake in China) are directly taken from "PEER earthquake ground database"[1)]. The key information of these three selected seismic waves is listed in Table 2. The acceleration spectra and the isolation efficiency are shown in Figs. 8-10. It is observed that the novel NPR seismic metamaterial exhibited superior isolation performances. For the Kobe earthquake (as shown in Fig. 8), whose main frequency is located within 0.60 Hz-2.87 Hz, over 80.5% acceleration amplitude decrease has been observed. For the Tsukidate earthquake (as shown in Fig. 9), whose main frequency is located within 1.80 Hz-3.90 Hz, the attenuation ratio exceeds 78% in acceleration amplitude. For the Jiashi earthquake, which has a wide frequency range of 2.1 Hz-21.7 Hz, the attenuation ratio exceeds 71.9% is observed. As shown in Figs. 8(d), 9(d), and 10(d), we can clearly find that the initial isolation frequency for the three real seismic waves is around 0.65 Hz, which is consistent with the frequency bandgap of

1) https://ngawest2.berkeley.edu/.

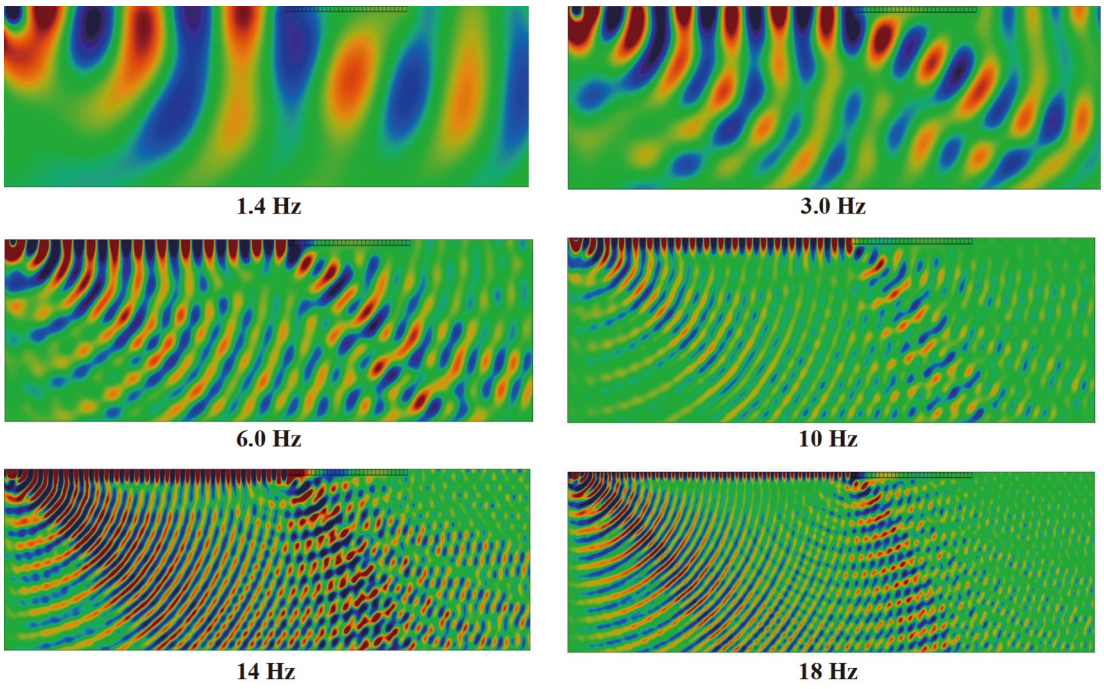


**Figure 7** Vertical displacement fields at different input frequencies and mode conversion of Rayleigh wave to the bulk shear wave propagating deep into the ground.

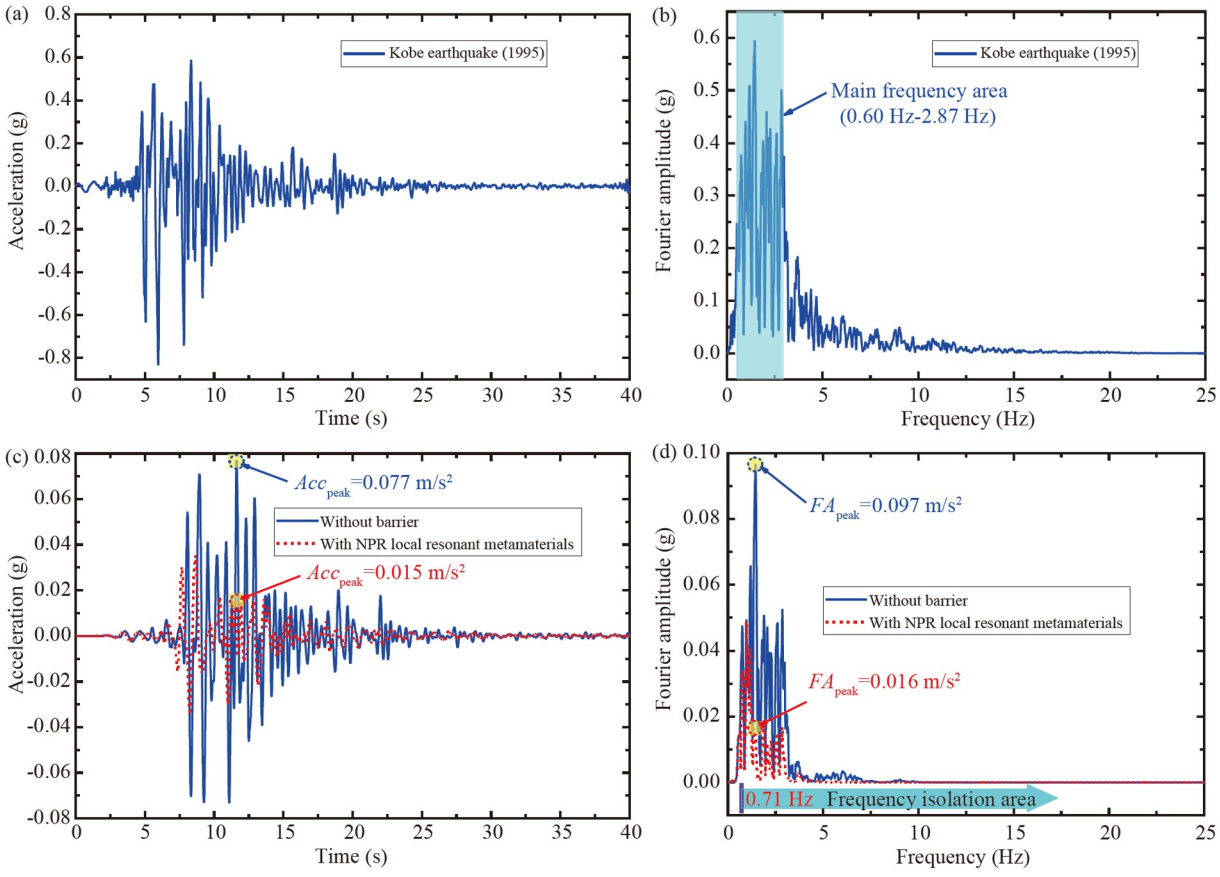


**Figure 8** Kobe earthquake acceleration spectrum and the isolation effect. (a) Acceleration-time history curves of Kobe earthquake; (b) acceleration spectra of Kobe wave; (c) time-domain acceleration responses with and without NPR locally resonant metamaterial; (d) acceleration spectra with and without NPR locally resonant metamaterial.

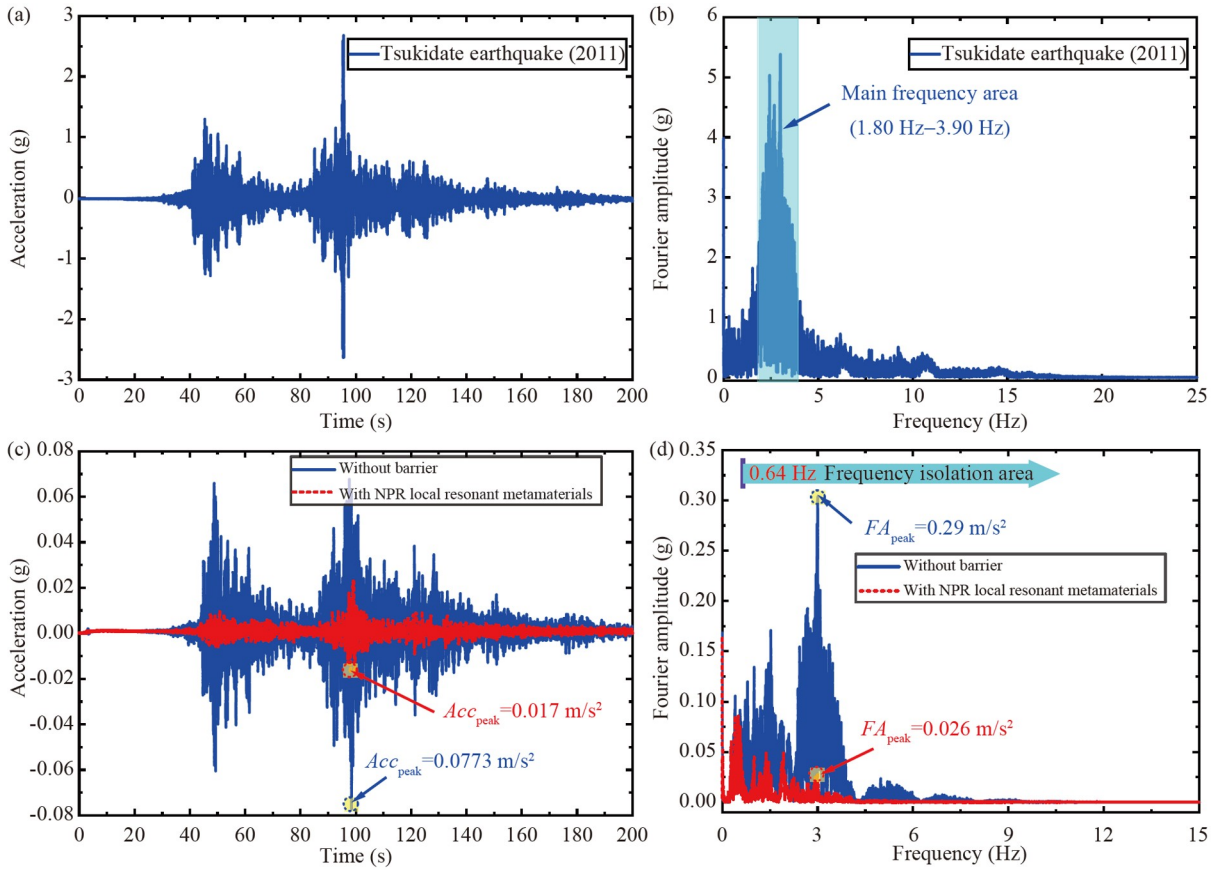


**Figure 9** Tsukidate earthquake acceleration spectrum and the isolation effect. (a) Acceleration-time history curves of Tsukidate earthquake; (b) acceleration spectra of Tsukidate wave; (c) time-domain acceleration responses with and without NPR locally resonant metamaterial; (d) acceleration spectra with and without NPR locally resonant metamaterial.

**Table 2** Properties of earthquake excitation

| Earthquake | Time | Peak (g) | Duration (s) | Arias intensity (m/s) | Mag |
|---|---|---|---|---|---|
| Kobe earthquake in Japan | 1995 | 0.826 | 40 | 8.4 | 6.9 |
| Tsukidate earthquake in Japan | 2011 | 1.268 | 300 | 6.6 | 9.0 |
| Jiashi earthquake in China | 1997 | 0.081 | 60 | 0.2 | 5.93 |

the NPR locally resonant seismic metamaterial proposed in this work.

## 4. Conclusions

The traditional local resonator seismic metamaterial does not consider energy-absorbing characteristics, while the NPR metamaterial has fascinating energy-absorbing characteristics. Therefore, combining the characteristics of the locally resonant seismic metamaterials and NPR metamaterial, we proposed a new NPR locally resonant seismic metamaterial. The sound cone technique is used to identify the surface wave, which is verified with the energy method. Subsequently, the generation mechanism of the frequency bandgap, the influence of NPR material on frequency bandgap, the isolation effectiveness of NPR seismic metamaterials, and time domain analysis are discussed in detail using COMSOL Multiphysics. The conclusions obtained in this work are as follows:

(1) The ultra-low and ultra-wide frequency bandgap of 0.65 Hz-18.9 Hz with the resonators arranged seriate is obtained due to the locally resonant and energy absorption by the NPR locally resonant seismic metamaterial proposed in this work. The fascinating isolation effect is realized by transforming the surface wave into the bulk wave. The generation mechanism of frequency bandgap based on the local resonant is verified by the model analysis.

(2) The distance between each resonator has a significant influence on both the lower and upper bound frequencies, i.e., the lower and upper bound frequencies for distance of 0 m are respectively 0.65 Hz and 18.9 Hz, while the lower and upper bound frequencies are 3.64 Hz and 10.7 Hz for distance of 1.3 m. Indicating that with increasing the dis-

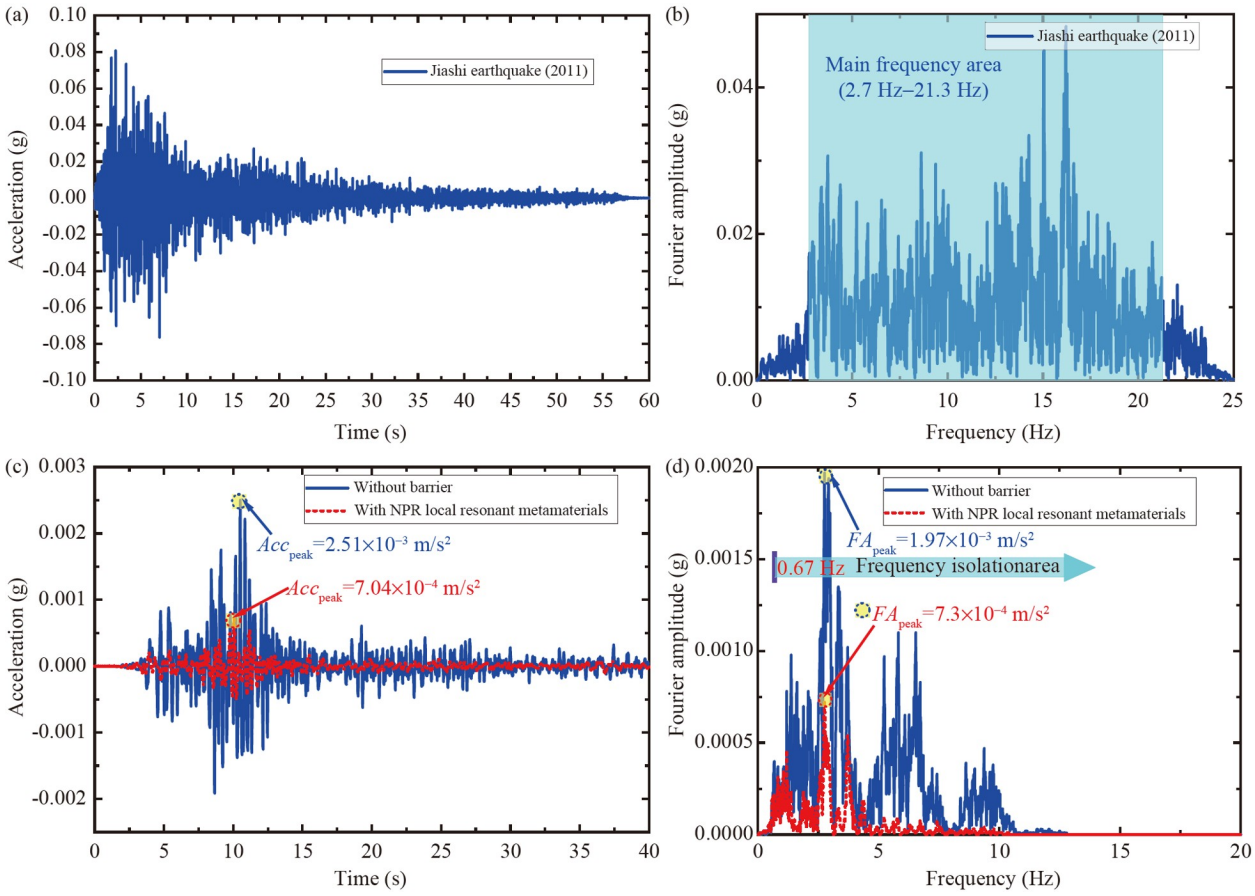


**Figure 10** Jiashi earthquake acceleration spectrum and the isolation effect. (a) Acceleration-time history curves of Jiashi earthquake; (b) acceleration spectra of Jiashi wave; (c) time-domain acceleration responses with and without NPR locally resonant metamaterial; (d) acceleration spectra with and without NPR locally resonant metamaterial.

tance of each resonator, the UBF decreases gradually, while the LBF increases when the distance reaches a critical value.

(3) The Poisson ratio, mass density, and elastic modulus of NPR bearing have a remarkable impact on the frequency bandgap, especially on the UBF, such as the UBF decreases from 18.7 Hz to 11.6 Hz with increasing the NPR value. In practical engineering, the NPR bearing with low Poisson, small mass density, and high elastic modulus is suggested to design the NPR local resonant seismic metamaterial to generate the board frequency bandgap.

(4) The time domain analysis indicates that the proposed NPR local resonant seismic metamaterial structure has a promising application in isolating the real earthquake waves with the main frequency from 0.65 Hz-20 Hz, which is consistent with the frequency bandgap of the seismic metamaterial proposed in this work.

The contribution of this work provides a new idea for designing the local resonant seismic metamaterial to protect civil infrastructures from the damage of seismic waves. While the theoretical research and the saturated soil media on this new seismic metamaterial need to be further considered in future work.

## Data availability

Data will be made available on request.

***Conflict of interest*** *On behalf of all authors, the corresponding author states that there is no conflict of interest.*

***Author contributions*** ***Haibin Ding****: Conceptualization, Data curation, Formal analysis, Funding acquisition, Investigation, Methodology, Writing – original draft, Writing – review & editing.* ***Nianyong Huang****: Funding acquisition, Data curation, Investigation, Methodology, Writing – review & editing.* ***Muhammad****: Conceptualization, Data curation, Investigation, Methodology, Validation, Writing – review & editing.* ***Changjie Xu:*** *Conceptualization, Investigation, Methodology, Writing – review & editing.* ***Lihong Tong:*** *Conceptualization, Investigation, Methodology, Writing – review & editing.*

***Acknowledgements*** *The work was supported by the National Natural Science Foundation (Grant Nos. 52208344 and 52278350), the Natural Science Foundation of Jiangxi Province (Grant Nos. 20224BAB214068 and 20212BDH81034), Education Department of Jiangxi Province (Grant No. GJJ2200673) and Open Project of State Key Laboratory (Grant No. HJGZ2022204).*

1 M. Zhang, and Y. Jin, Building damage in Dujiangyan during Wenchuan earthquake, Earthq. Eng. Eng. Vib. **7**, 263 (2008).
2 Z. A. Kazmi, and K. Konagai, Co-seismic stress changes and damage to tunnels in the 23 October 2004 Mid-Niigata Prefecture earthquake,

Can. Geotech. J. **55**, 736 (2018).
3 M. Naddaf, Turkey-Syria earthquake: What scientists know, Nature **614**, 398(2023).
4 G. Y. Gao, Z. Y. Li, C. Qiu, and Z. Q. Yue, Three-dimensional analysis of rows of piles as passive barriers for ground vibration isolation, Soil Dyn. Earthq. Eng. **26**, 1015 (2006).
5 G. Gao, J. Chen, X. Gu, J. Song, S. Li, and N. Li, Numerical study on the active vibration isolation by wave impeding block in saturated soils under vertical loading, Soil Dyn. Earthq. Eng. **93**, 99 (2017).
6 R. S. Jangid, Optimum lead-rubber isolation bearings for near-fault motions, Eng. Struct. **29**, 2503 (2007).
7 Muhammad, and C. W. Lim, From photonic crystals to seismic metamaterials: A review via phononic crystals and acoustic metamaterials, Arch. Comput. Method. Eng. **29**, 1137 (2022).
8 Z. Cheng, and Z. Shi, Novel composite periodic structures with attenuation zones, Eng. Struct. **56**, 1271 (2013).
9 H. H. Huang, and C. T. Sun, Wave attenuation mechanism in an acoustic metamaterial with negative effective mass density, New J. Phys. **11**, 013003 (2009).
10 A. Bhatt, and A. Banerjee, Double attenuation peaks in metamaterial with simultaneous negative mass and stiffness, Phys. Lett. A **443**, 128201 (2022).
11 H. Danawe, and S. Tol, Experimental realization of negative refraction and subwavelength imaging for flexural waves in phononic crystal plates, J. Sound Vib. **518**, 116552 (2022).
12 H. Yang, and L. Ma, Design and characterization of axisymmetric auxetic metamaterials, Compos. Struct. **249**, 112560 (2020).
13 Z. Tao, X. Ren, A. G. Zhao, L. Sun, Y. Zhang, W. Jiang, D. Han, X. Y. Zhang, and Y. M. Xie, A novel auxetic acoustic metamaterial plate with tunable bandgap, Int. J. Mech. Sci. **226**, 107414 (2022).
14 S. Brûlé, E. H. Javelaud, S. Enoch, and S. Guenneau, Experiments on seismic metamaterials: Molding surface waves, Phys. Rev. Lett. **112**, 133901 (2014).
15 X. Pu, and Z. Shi, Periodic pile barriers for Rayleigh wave isolation in a poroelastic half-space, Soil Dyn. Earthq. Eng. **121**, 75 (2019).
16 S. Amanat, R. Rafiee-Dehkharghani, M. Bitaraf, and D. Bansal, Analytical and numerical investigation of finite and infinite periodic lattices for mitigation of seismic waves in layered grounds, Int. J. Eng. Sci. **173**, 103655 (2022).
17 M. Miniaci, A. Krushynska, F. Bosia, and N. M. Pugno, Large scale mechanical metamaterials as seismic shields, New J. Phys. **18**, 083041 (2016).
18 J. Huang, W. Liu, and Z. Shi, Surface-wave attenuation zone of layered periodic structures and feasible application in ground vibration reduction, Constr, Build, Mater. **141**, 1 (2017).
19 J. Bao, Z. Shi, and H. Xiang, Dynamic responses of a structure with periodic foundations, J. Eng. Mech. **138**, 761 (2012).
20 Z. B. Cheng, and Z. F. Shi, Composite periodic foundation and its application for seismic isolation, Earthq. Eng. Struct. Dyn. **47**, 925 (2018).
21 A. Palermo, S. Krödel, A. Marzani, and C. Daraio, Engineered metabarrier as shield from seismic surface waves, Sci. Rep. **6**, 39356 (2016).
22 Muhammad, C. W. Lim, and K. Kamil Żur, Wide Rayleigh waves bandgap engineered metabarriers for ground born vibration attenuation, Eng. Struct. **246**, 113019 (2021).
23 A. Khelif, Y. Achaoui, S. Benchabane, V. Laude, and B. Aoubiza, Locally resonant surface acoustic wave band gaps in a two-dimensional phononic crystal of pillars on a surface, Phys. Rev. B **81**, 214303 (2010).
24 Q. J. Du, Y. Zeng, Y. Xu, H. W. Yang, and Z. X. Zeng, H-fractal seismic metamaterial with broadband low-frequency bandgaps, J. Phys. D **51**, 105104 (2018).
25 Muhammad, C. W. Lim, and J. N. Reddy, Built-up structural steel sections as seismic metamaterials for surface wave attenuation with low frequency wide bandgap in layered soil medium, Eng. Struct. **188**, 440 (2019).
26 A. Colombi, D. Colquitt, P. Roux, S. Guenneau, and R. V. Craster, A seismic metamaterial: The resonant metawedge, Sci. Rep. **6**, 27717 (2016).
27 A. Colombi, P. Roux, S. Guenneau, P. Gueguen, and R. V. Craster, Forests as a natural seismic metamaterial: Rayleigh wave bandgaps induced by local resonances, Sci. Rep. **6**, 19238 (2016).
28 Muhammad, and C. W. Lim, Natural seismic metamaterials: The role of tree branches in the birth of Rayleigh wave bandgap for ground born vibration attenuation, Trees **35**, 1299 (2021).
29 Muhammad, T. Wu, and C. W. Lim, Forest trees as naturally available seismic metamaterials: Low frequency Rayleigh wave with extremely wide bandgaps, Int. J. Str. Stab. Dyn. **20**, 2043014 (2020).
30 C. He, S. Zhou, X. Li, H. Di, and X. Zhang, Forest trees as a natural metamaterial for surface wave attenuation in stratified soils, Constr. Build. Mater. **363**, 129769 (2023).
31 A. Palermo, M. Vitali, and A. Marzani, Metabarriers with multi-mass locally resonating units for broad band Rayleigh waves attenuation, Soil Dyn. Earthq. Eng. **113**, 265 (2018).
32 R. Zaccherini, A. Colombi, A. Palermo, V. K. Dertimanis, A. Marzani, H. R. Thomsen, B. Stojadinovic, and E. N. Chatzi, Locally resonant metasurfaces for shear waves in granular media, Phys. Rev. Appl. **13**, 034055 (2020).
33 J. Lou, X. Fang, H. Fan, and J. Du, A nonlinear seismic metamaterial lying on layered soils, Eng. Struct. **272**, 115032 (2022).
34 A. Palermo, B. Yousefzadeh, C. Daraio, and A. Marzani, Rayleigh wave propagation in nonlinear metasurfaces, J. Sound Vib. **520**, 116599 (2022).
35 G. Imbalzano, P. Tran, T. D. Ngo, and P. V. S. Lee, A numerical study of auxetic composite panels under blast loadings, Compos. Struct. **135**, 339 (2016).
36 F. Ebrahimian, Z. Kabirian, D. Younesian, and P. Eghbali, Auxetic clamped-clamped resonators for high-efficiency vibration energy harvesting at low-frequency excitation, Appl. Energy **295**, 117010 (2021).
37 W. J. G. Ferguson, Y. Kuang, K. E. Evans, C. W. Smith, and M. Zhu, Auxetic structure for increased power output of strain vibration energy harvester, Sens. Actuat. A-Phys. **282**, 90 (2018).
38 M. S. H. Al-Furjan, C. Yin, X. Shen, R. Kolahchi, M. S. Zarei, and M. H. Hajmohammad, Energy absorption and vibration of smart auxetic FG porous curved conical panels resting on the frictional viscoelastic torsional substrate, Mech. Syst. Signal Process. **178**, 109269 (2022).
39 B. Ungureanu, Y. Achaoui, S. Enoch, S. Brûlé, and S. Guenneau, Auxetic-like metamaterials as novel earthquake protections, EPJ Appl. Metamaterials **2**, 17 (2016).
40 T. T. Huang, X. Ren, Y. Zeng, Y. Zhang, C. Luo, X. Y. Zhang, and Y. M. Xie, Based on auxetic foam: A novel type of seismic metamaterial for Lamb waves, Eng. Struct. **246**, 112976 (2021).
41 L. Tong, Y. Yu, W. Hu, Y. Shi, and C. Xu, On wave propagation characteristics in fluid saturated porous materials by a nonlocal Biot theory, J. Sound Vib. **379**, 106 (2016).
42 L. H. Tong, H. B. Ding, J. W. Yan, C. Xu, and Z. Lei, Strain gradient nonlocal Biot poromechanics, Int. J. Eng. Sci. **156**, 103372 (2020).
43 X. Wang, S. Wan, Y. Nian, P. Zhou, and Y. Zhu, Periodic in-filled pipes embedded in semi-infinite space as seismic metamaterials for filtering ultra-low-frequency surface waves, Constr. Build. Mater. **313**, 125498 (2021).
44 M. Badreddine Assouar, and M. Oudich, Dispersion curves of surface acoustic waves in a two-dimensional phononic crystal, Appl. Phys. Lett. **99**, 123505 (2011).
45 X. Pu, and Z. Shi, A novel method for identifying surface waves in periodic structures, Soil Dyn. Earthq. Eng. **98**, 67 (2017).
46 Y. Zeng, P. Peng, Q. J. Du, Y. S. Wang, and B. Assouar, Subwavelength seismic metamaterial with an ultra-low frequency bandgap, J. Appl. Phys. **128**, 014901 (2020).
47 C. F. Zhao, C. Q. Chen, C. Zeng, W. Bai, and J. W. Dai, Novel periodic pile barrier with low-frequency wide bandgap for Rayleigh waves, Int. J. Mech. Sci. **243**, 108006 (2023).
48 X. Pu, A. Palermo, Z. Cheng, Z. Shi, and A. Marzani, Seismic

metasurfaces on porous layered media: Surface resonators and fluid-solid interaction effects on the propagation of Rayleigh waves, Int. J. Eng. Sci. **154**, 103347 (2020).
49 F. Zeighami, A. Palermo, and A. Marzani, Rayleigh waves in locally resonant metamaterials, Int. J. Mech. Sci. **195**, 106250 (2021).
50 Z. Chen, G. Wang, and C. W. Lim, Artificially engineered metaconcrete with wide bandgap for seismic surface wave manipulation, Eng. Struct. **276**, 115375 (2023).
51 Y. Zhang, X. Ren, X. Y. Zhang, T. T. Huang, L. Sun, and Y. M. Xie, A novel buckling-restrained brace with auxetic perforated core: Experimental and numerical studies, Eng. Struct. **249**, 113223 (2021).
52 Y. Zhang, L. Sun, X. Ren, X. Y. Zhang, Z. Tao, and Y. M. Xie, Design and analysis of an auxetic metamaterial with tuneable stiffness, Compos. Struct. **281**, 114997 (2022).

# 负泊松比局域共振型地震超材料隔震屏障

丁海滨, 黄年勇, Muhammad, 徐长节, 童立红

**摘要** 近几十年来, 地震超材料在保护土木工程基础设施免受地震破坏方面的应用受到了广泛关注. 尤其是局域共振地震超材料的提出, 为使用小尺寸隔离屏障实现低频地震波隔离提供了可能. 然而, 以往的研究中, 未考虑局域共振地震超材料的能量吸收特性. 利用负泊松比(NPR)超材料良好的能量吸收特性, 将局域共振的地震超材料与NPR超材料结合, 创造性地设计了一种新的地震超材料结构, 以隔离地震波. 采用声锥技术结合透射谱从混合波中识别表面波. 详细讨论了频率带隙的产生机制和所提出的地震超材料的隔震效果. 结果表明, 超材料结构在0.65 Hz-18.9 Hz范围内产生的超低、超宽频带隙主要是由于地震超材料结构的局域共振和能量吸收所致, 通过将表面波转换为体波获得了良好的隔振效果. 随着每个谐振器之间距离的增加, 频率带隙变窄. 此外, NPR垫层的泊松比、密度和弹性模量等力学性能对频率带隙有显著影响, 特别是对上限频率(UBF)的影响更大. 在实际工程中, 负泊松比局域共振地震超材料结构的设计建议选择负泊松比值、密度及弹性模量均较小的负泊松比材料. 对实际地震波的时域分析表明, 该材料在隔离超低、超宽频率地震波方面具有良好的应用前景, 隔振效果大于70%. 这项工作为局域共振地震超材料隔离低频地震波提供了一种新的设计思想.